Materials Today 88 (2025) 1–11

Contents lists available at ScienceDirect

Materials Today

journal homepage: www.elsevier.com/locate/mattod

Short Communication (mid green)

Six key variables in 2D MXenes for hydrogen evolution electrocatalysis

Anupma Thakur [a], Nithin Chandran B.S. [a], Brian C. Wyatt [a], Annabelle Bedford [a], Mostafa Dadashi Firouzjaei [b], Krutarth Kamath [a], Muhammad Sharif Uddin [a], Babak Anasori [a,c,*]

[a] School of Materials Engineering, Purdue University, West Lafayette, IN 47907, the United States of America
[b] Department of Civil, Construction, and Environmental Engineering, University of Alabama, Tuscaloosa, AL 35487, the United States of America
[c] School of Mechanical Engineering, Purdue University, West Lafayette, IN 47907, the United States of America

ARTICLE INFO

Keywords:
MXenes
Electrocatalysis
Double transition metal
Hydrogen
Energy

ABSTRACT

MXenes, with their $M_{n+1}X_nT_x$ chemical formula, have diverse chemical compositions and structures among two-dimenionsal (2D) materials. MXenes have emerged as potential electrocatalysts for hydrogen evolution reaction (HER) due to their abundant active sites on the 2D basal planes and tunable electronic properties. MXenes with two or more transition metals are growing subfamilies of MXenes, including random solid solutions, ordered double-metal, and multi-metal (four or more metal) MXenes. Computational studies indicate that ordered double transition metal (DTM) MXenes (o-MXenes) offer superior catalytic HER performance compared to mono-transition metal MXenes. In this article, we first present six key factors that play critical roles in the tunability and control of the HER performance of MXenes, including composition (M, X, and T_x), the thickness of 2D flake (number of atomic layers), lateral flake dimensions, surface adatoms, and intercalating ions, atomic defects (e.g., vacancies), and heteroatom doping. We then systematically evaluate the effect of transition metals (M) on MXenes HER activity by analyzing 14 single-metal and ordered DTM MXenes, including four M_2CT_x as Mo_2CT_x, V_2CT_x, Nb_2CT_x, Ti_2CT_x, four $M_3C_2T_x$ as $Ti_3C_2T_x$, $Mo_2TiC_2T_x$, $Cr_2TiC_2T_x$, $W_2TiC_2T_x$ and six $M_4C_3T_x$ as $V_4C_3T_x$, $Nb_4C_3T_x$, $Ta_4C_3T_x$, $Mo_2Ti_2C_3T_x$, $Mo_2Nb_2C_3T_x$ and $Mo_2V_2C_3T_x$. By focusing on the role of M in MXenes, with Ti, V, Cr, Nb, Mo, Ta, and W as their inner and outer planes, we provide a comprehensive understanding of their effects on HER activity. Among all screened MXenes, $W_2TiC_2T_x$ MXene shows the lowest HER overpotential of ~149 mV at 10 mA/cm^2 under acidic conditions, which could be attributed to the active W-basal plane. This work provides insights into the interplay of six compositional and structural factors in MXene-based HER and highlights the critical influence of transition metal selection in guiding the development of high-performance MXene electrocatalysts.

Introduction

Since 2016, hydrogen evolution reaction (HER) has become one of the key areas of research and potential applications of the two-dimensional (2D) transition metal carbides, nitrides, or carbonitrides, known as MXenes [1,2]. Discovered in 2011, MXenes are a growing family of 2D materials mostly derived from bulk-layered $M_{n+1}AX_n$ phases (where n = 1–4) which consist of n + 1 layers of one or more transition metals (M, typically from groups 4–6), interleaved with X layers, carbon (C), nitrogen (N) or both (CN), and an A group element (usually from groups 13–16) [3,4]. Their compositions can be tuned by the use of different transition metals of groups 4 to 6 (M: Ti, Zr, Hf, V, Nb, Ta, Cr, Mo, and W), the sublattice X (carbon or nitrogen), and the surface terminations (T_x) can be different elements of groups 16 and 17 of the periodic table, hydroxyl, and some organic compounds. The structure can be controlled by changing the number of atomic layers (thickness) with n = 1–4. Most of these tunabilities come from MXenes' precursors. MXenes are mainly made via top-down methods and derived from the selective etching of the A element in layered MAX phases (Fig. 1**a**) using suitable etchants. Fig. 1**b** shows the elements reported in MAX phases and highlights their chemical diversity [5].

The synthesis of MXenes involves selectively etching the A-group layer from the MAX phase using acid-assisted etching, molten salt etching, or electrochemical etching [3]. The relatively weak metallic

* Corresponding author.
E-mail address: banasori@purdue.edu (B. Anasori).

https://doi.org/10.1016/j.mattod.2025.06.018
Received 17 March 2025; Received in revised form 14 May 2025; Accepted 8 June 2025
Available online 19 June 2025

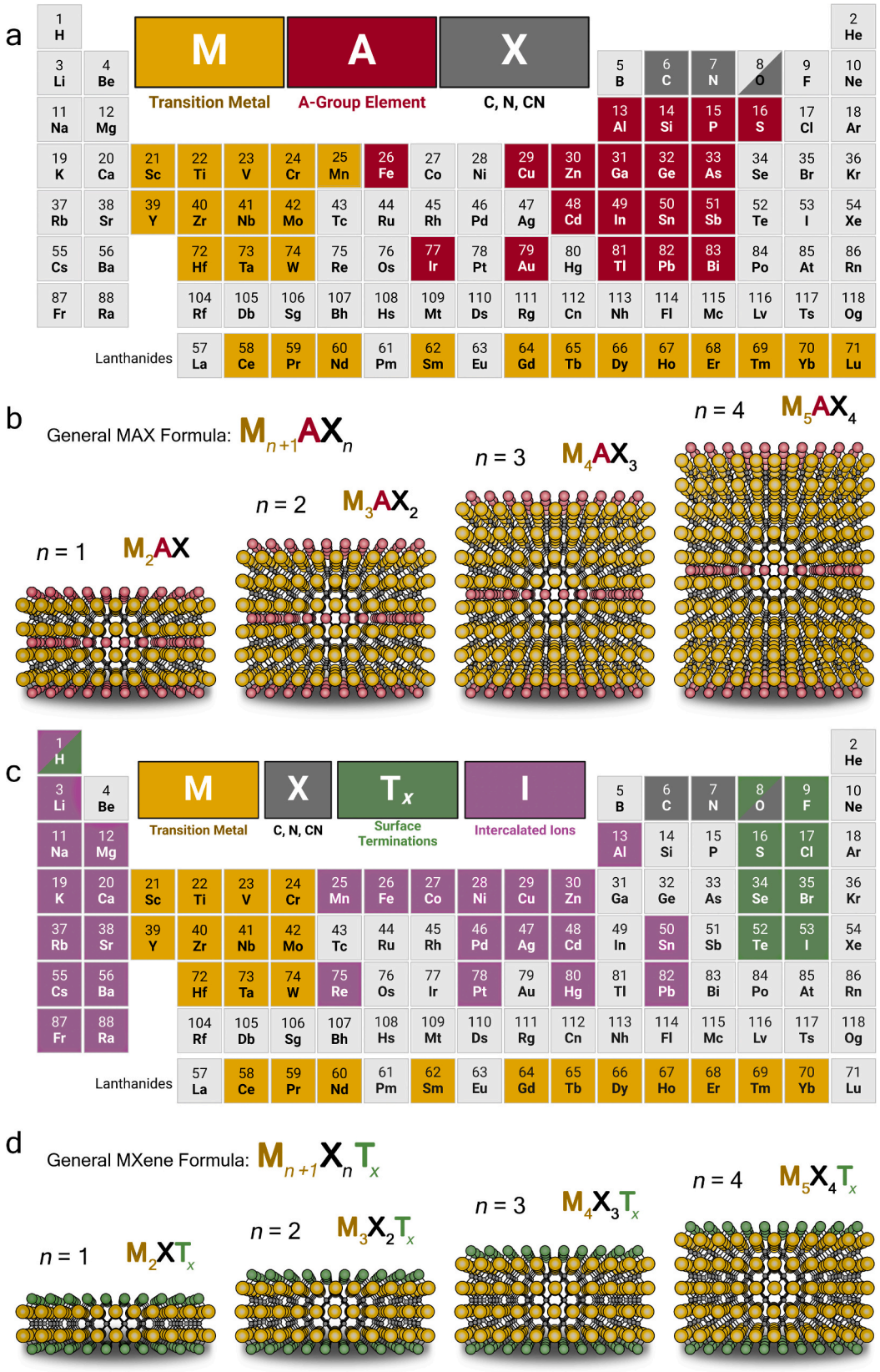

Fig. 1. Compositional diversity of MAX and MXenes. **a** Schematic of four typical MAX phases such as M_2AX, M_3AX_2, M_4AX_3 and M_5AX_4. **b** Periodic table showing the elements used to synthesize MAX phases to date (gold background are reported as M layers in MAX phases, red background are the A elements that can potentially be selectively etched to make MXenes, grey background represent the X element in the MAX phase). **c** MXenes synthesized after elective etching of A layers (red atoms) and formation of surface terminations (green atoms). **d** Periodic table showing elements reported to synthesize MXenes from their parent MAX phases to date (gold background is only reported as M layers in MXenes, grey background represents the X element in the MXenes, green background represents the surface terminations,

and purple background represents the intercalated ions). (For interpretation of the references to colour in this figure legend, the reader is referred to the web version of this article.)

bond between M−A layers compared with the stronger mixed ionic/covalent nature of the M−X makes it possible to selectively etch the A-group layer to separate the $M_{n+1}X_n$ layers from the MAX phase [3]. Upon selective etching, undercoordinated transition metals are saturated with functional species (T_x), commonly –OH, −O, −F, and −Cl, resulting in four $M_{n+1}X_nT_x$ MXene structures shown in Fig. 1**c** [6]. Fig. 1**d** shows the periodic table representation of elements for the reported MXenes to date along with the elements that have been intercalated.

The unique properties of MXenes include highly tunable chemistry, metal-like electrical conductivity (~24000 S/cm for $Ti_3C_2T_x$), mechanical stiffness (480 GPa stiffness for $Ti_3C_2T_x$ single flake), and thermal stability (up to 900 °C for $Ti_3C_2T_x$) in inert environments [6–8]. These characteristics make MXenes potential 2D materials for various energy applications ranging from supercapacitors to electrocatalysts [2,9,10]. MXenes offer a wide range of compositional tailoring, structural tunability, and an intriguing combination of properties, making them a rapidly growing area of research (**ESI**, Fig. S1). Therefore, it is essential to classify MXene compositions, understand synthesis

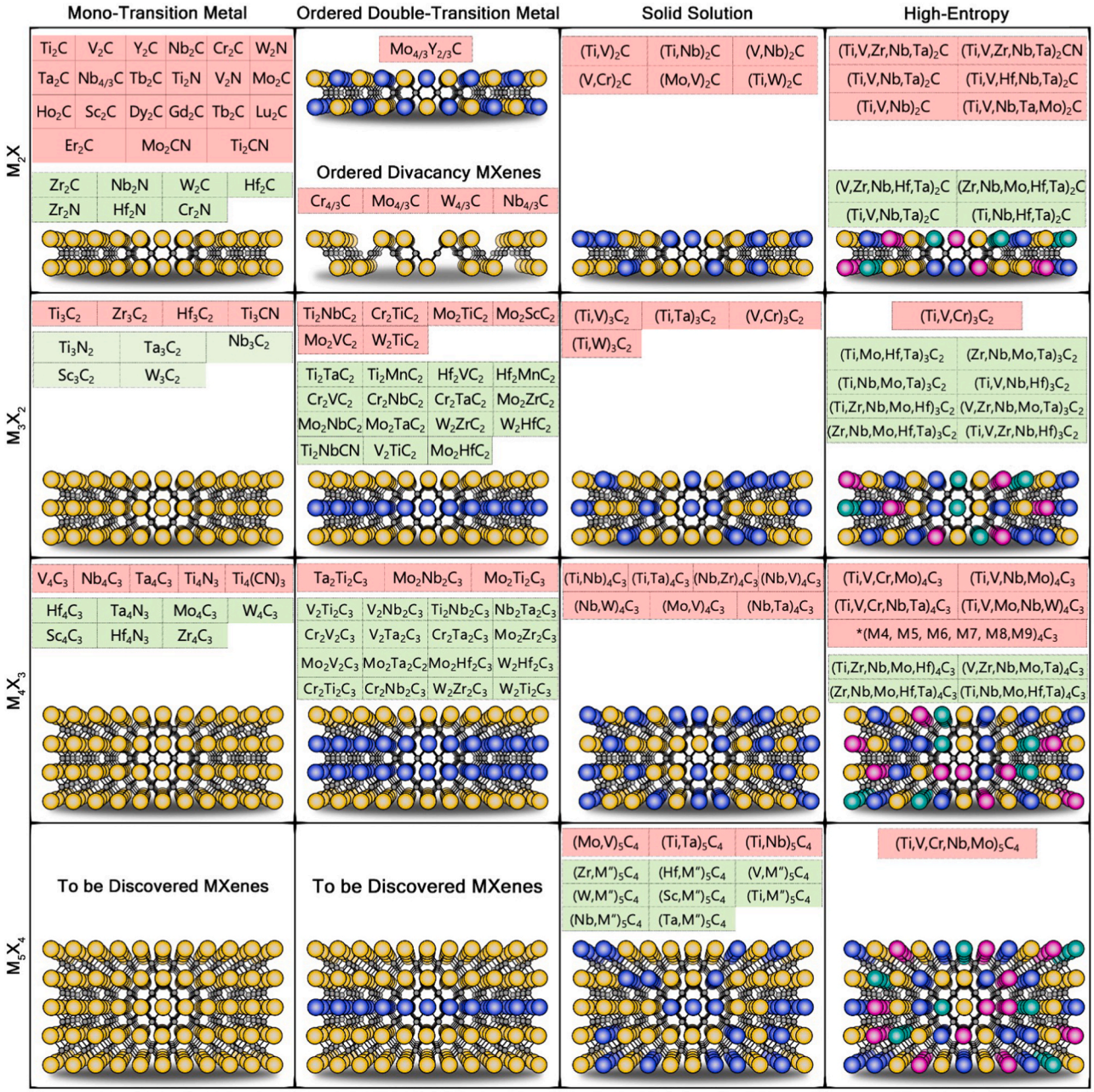

Fig. 2. MXene compositions reported to date. The four rows represent the types of MXenes based on the number of layers such as M_2X, M_3X_2, M_4X_3, and M_5X_4. The first column shows the mono-transition metal MXenes. The second column shows ordered DTM MXenes and ordered divacancy MXenes. The third column shows solid solution DTM MXenes and the fourth column shows high-entropy MXenes. This table includes experimentally (red text background) and theoretically (green text background) explored MXene compositions. In the row M_4X_3, * represents ~35 new MXenes recently discovered with transition metals ranging from 4 to 9. The surface terminations T_x are not shown for simplicity. (For interpretation of the references to colour in this figure legend, the reader is referred to the web version of this article.)

strategies, and tailor their properties for targeted applications.

In this article, we first provide a summary of the MXene compositions reported to date, their synthesis routes, and the big picture of their applications. We then focus on MXenes as a promising group of electrocatalytic materials and discuss six key factors that control MXenes HER kinetics. One of the key factors in MXenes HER activities is the transition metal compositions in MXenes. To fully demonstrate the effect of the transition metal composition, we end this article by presenting a systematic case study of HER performance of 14 different MXenes, with Ti, V, Cr, Nb, Mo, Ta, and W as their inner and outer planes. To avoid any discrepancies, we synthesized all 14 MXenes in our lab and tested them under the same conditions. This systematic study enables us to minimize synthesis and manufacturing variables and focus on the tunability of MXene by changing their transition metals. An ordered transition metal MXenes with W occupying 70 at% of the outer M and Ti occupying the inner M in a $M_3C_2T_x$ outperformed all tested MXenes for HER. This article guides the future MXene HER research in systematic studies to design the most effective 2D electrocatalysts.

MXene compositions, synthesis, and applications

The expansion of MXene compositions has been mainly done by manipulating their transition metal layer compositions and structures. Mono-transition metals (mono-Ms) and random bi-metallic solid solutions to ordered bi-metallic MXenes, known as out-of-plane and in-plane ordered double transition metal (DTM) MXenes, also known as o-MXenes and i-MXenes, were discovered in 2015 [11] and 2018 [12], respectively. The $M_5C_4T_x$ MXenes with five layers of metals were discovered in 2019 [13] and high-entropy (HE) MXenes, with four or more metals, were discovered in 2021 [14]. The mono-M MXenes have been reported in the $n = 1$–3 structures (M_2X, M_3X_2, and M_4X_3), while MXenes with two or more metals cover all four structures ($n = 1$–4) as shown in Fig. 2.

In random solid solution MXenes, the randomness usually allows more flexibility with the ratio of the two M elements [15]. Many random solid solution MXenes are shown to be stable in a wide range of the two M elements (M1:M2) molar ratios, such as in $(Ti,V)_2CT_x$, $(Ti,Nb)_2CT_x$ and $(V,Nb)_2CT_x$ [16]. In contrast, the ordered DTM MXenes, in which two transition metals (M' and M'') occupy separate atomic planes in the MXene 2D flake, are very sensitive to the outer metal: inner metal (M': M'') molar ratios. For example, in an ordered $Mo_2TiC_2T_x$ structure, a slight change from the Mo:Ti 2:1 ratio in the starting powder mixture in synthesizing the precursor does not lead to the formation of its MAX precursor phase (Fig. 2) [15,17]. Considering in-plane ordered DTM MXenes (e.g., $Mo_{4/3}Y_{2/3}CT_x$ [12], the minority transition metal (e.g., Y in $Mo_{4/3}Y_{2/3}CT_x$) occupies specific rows within the basal plane of the majority metal (Mo), with Y slightly shifted toward the outer plane. During MXene synthesis, the Y metal can be etched along with Al from the precursor phase, forming divacancy MXenes (Fig. 2).

Out-of-plane ordered MXene is only reported in the $M_3C_2T_x$ and

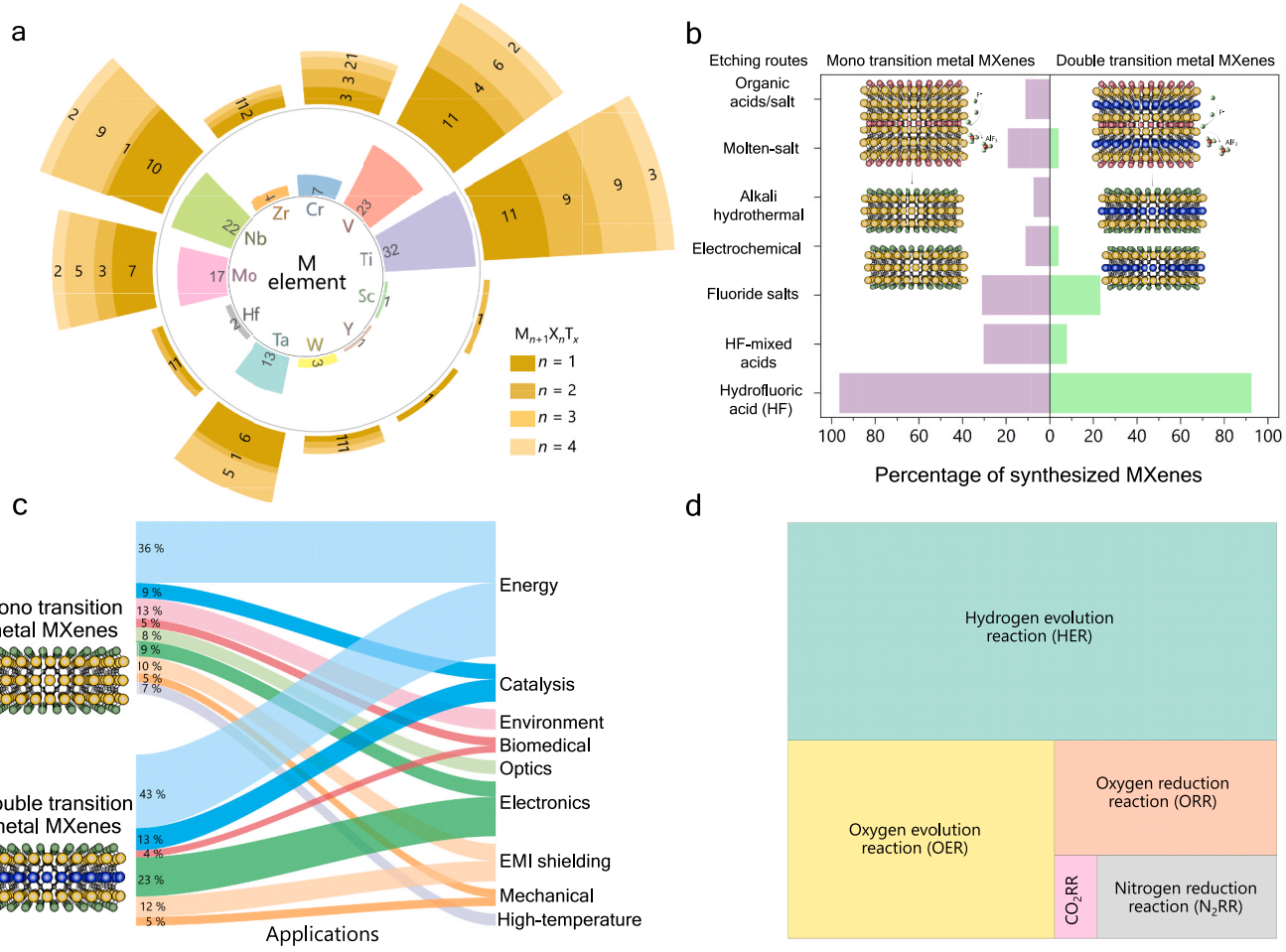

Fig. 3. MXene synthesis and applications reported to date. **a** Radial plot shows an overview of the number of the M−site occupancy (inner plot) and layer thickness (outer plot) of the synthesized MXenes to date. **b** Bar chart shows the percentage of reported mono-transition metal and DTM MXenes synthesized using wet-chemical etching routes. **c** Alluvial chart shows the percentage of publications in each explored application of mono-transition metal and DTM MXenes to the total number of publications. **d** Tree map represents the distribution of MXenes and their hybrids in electrocatalysis.

$M_4C_3T_x$, in which the outer metal planes differ from the inner plane metals. For example, Ti can be sandwiched between layers of Cr or Mo in $Cr_2TiC_2T_x$, and $Mo_2TiC_2T_x$ [15]. To date, nine out-of-plane ordered MXenes are reported, $Mo_2TiC_2T_x$ [11], $Mo_2ScC_2T_x$ [18], $Cr_2TiC_2T_x$ [19], $W_2TiC_2T_x$ [20], $Ti_2NbC_2T_x$ [21], $Mo_2VC_2T_x$ [22], $Mo_2Ti_2C_3T_x$ [11], $Mo_2Nb_2C_3T_x$ [23], and $Ta_2Ti_2C_3T_x$ [24]. Furthermore, high-entropy MXenes (Fig. 2), which incorporate four or more transition metals in equimolar proportions, have opened new directions for the growing MXene family [14,25].

To date, the M in all synthesized MXenes spans 11 different transition metals (Fig. 3**a**). Titanium (Ti) is the most explored transition metal for MXenes, followed by vanadium (V) and niobium (Nb). In Fig. 3**a,** we also map the distribution of these transition metals used in MXenes with different 2D flake thicknesses from $n = 1$ (M_2XT_x) to $n = 4$ ($M_{5X4}T_x$), highlighting their structural diversity. Besides changing the M (or X) to tune the MXene compositions, the surface chemistry of MXenes can be tailored by employing different etching and delamination pathways. Wet-chemical etching routes using hydrofluoric acid (HF), mixed acids (e.g., HF and hydrochloric acid (HCl)), use of salts mixed with acids (e.g., the minimally intensive layer delamination (MILD) approach using fluoride salts and HCl), as well as electrochemical etching, alkali-assisted hydrothermal methods, molten salt techniques, and organic acids/salts are employed for synthesizing MXenes (Fig. 3**b**). While the wet chemical etching methods (including HF, HF-containing salts and HF-HCl result in mixed surface terminations, molten salts (e.g., NaCl, KCl, $CdCl_2$, $ZnCl_2$) form homogeneous halogen surface terminations during the etching process [26,27]. MAX phases can also be electrochemically etched in molten salt or ionic liquid to form MXenes [28]. In addition, MXenes are also synthesized via chemical vapor deposition (CVD) [29], direct synthesis routes [29] and gas-phase synthesis [30].

MXene etching methods effectively alter surface functionalities, defect concentration, intercalation and flake size, which all affect MXene performance [3,31]. Most MXenes are synthesized using HF (Fig. 3**b**), followed by mixed acids and MILD approaches. The MILD method and molten salt yield single-to-few-layer MXene flakes, suggesting the potential to explore less harsh etching methods. The alluvial plot in Fig. 3**c** illustrates the broad spectrum of applications of MXenes ranging from energy to biomedical sectors. For mono-M MXenes, the largest explored application area is energy storage and catalysis, accounting for ~ 45 % of their reported publications. In contrast, DTM MXenes have an even higher focus on energy storage and conversion technologies, comprising ~ 56 % of their applications. The increase in the number of published papers on DTM MXenes in the energy sector could be due to their higher compositional tunability (two metals), allowing for further tuning to excel in these areas and presenting the opportunity to expand tailored MXenes.

MXenes entire 2D basal planes are electrocatalytically active, which provides a platform for ongoing research focusing on catalysis for green energy production. The treemap in Fig. 3**d** shows the distribution of MXenes and their hybrids in catalytic applications spanning across HER (~52 %), oxygen evolution (~26 %), oxygen reduction (~13 %), nitrogen reduction (~7 %), and carbon dioxide reduction (~2 %). Despite several studies on HER of MXenes (Table S1**)**, only a very few studies have focused on the systematic tuning of MXene's surface chemistry for optimizing HER activity [32,33]. In the following sections, we will discuss the HER kinetics in MXenes and the six key factors that affect their potential as promising electrocatalysts for hydrogen production. One of the key factors in MXenes HER activities is the transition metal compositions in MXenes. To fully demonstrate the effect of the transition metal composition in MXenes, we present a systematic case study of HER performance of 14 different compositions, with Ti, V, Cr, Nb, Mo, Ta, and W as their inner and outer planes. To avoid any discrepancies, we made all the precursors and synthesized all 14 MXenes in our lab and tested them at the same conditions. This systematic study allows us to minimize synthesis and manufacturing variables and focus on the tunability of MXene by changing their transition metals.

Hydrogen evolution reaction kinetics in MXenes

MXenes' large surface area provides abundant active sites, metal-like electrical conductivity facilitates rapid electron transfer, hydrophilicity promotes efficient proton adsorption from the electrolyte, and tunable surface chemistry and chemical stability in various electrolytes ensure electrode durability [1,34,35]. Theoretical studies of MXenes for HER have focused on analyzing the thermodynamic descriptors, such as the hydrogen adsorption Gibbs free energy (ΔG_H) under standard conditions [36]. The optimal HER catalysis occurs when ΔG_H approaches 0 eV. The materials with $\Delta G_H < 0.2$ eV are considered HER-active, as this range minimizes kinetic barriers while preventing intermediate over-binding [36,37]. In HER electrocatalysis, the reaction proceeds through Volmer-Heyrovsky (VH) or Volmer-Tafel (VT) mechanisms [36]. Both mechanisms begin with a Volmer step, in which a proton (H^+) accepts an electron (e^-) and becomes adsorbed at an active site (*) on the catalyst surface, forming an adsorbed hydrogen atom (H*). The subsequent step distinguishes the two mechanisms: in the VH step, another H^+ and e^- react with H* to produce molecular hydrogen (H_2), regenerating the catalytic site. In contrast, the VT step involves the recombination of two H* atoms to form H_2, which then desorbs from the surface, regenerating the active site [38–40].

Given the large compositional space of MXenes, high-throughput studies with machine learning (ML) are required to identify the best HER-performing compositions. For example, a high-throughput spin-polarized DFT study using Perdew–Burke–Ernzerhof functionals compared the HER performance of mono-M MXenes and DTM MXenes and investigated the effect of both outer and inner metals (M' and M", respectively) [41]. The substitution of M'' in DTM MXenes notably reduces ΔG_H. After tailoring transition metals, the number of DTM MXenes exhibiting favorable $\Delta G_H < 0.2$ eV increased eightfold [41]. Selecting the right M' and M'' pairs in DTM MXenes can lower the activation energy barriers for hydrogen desorption reactions. For example, $Ti_2HfC_2O_2$ has a lower activation barrier (0.031 eV) for the Volmer–Heyrovsky pathway, indicating a more efficient hydrogen adsorption mechanism compared to $Ti_3C_2O_2$ (0.049 eV) [41].

Computational studies also provide insight into the HER trends by examining the electronic structures, hybridization of orbitals, and charge transfer properties, thus effectively tuning the hydrogen adsorption energy [41]. For hydrogen adsorption on the O-terminated surface, the H-1*s* and O-2*p* orbital hybridization leads to splitting into filled bonding (σ) and partially filled antibonding (σ*) orbitals, where higher σ* occupancy weakens binding strength. In DTM MXenes, the use of transition metals with different atomic radii in the inner sites (M'') [41] was shown to introduce lattice stress and strain. This affects the bond strengths and lengths between M−O and O-O ($d_{O–M}$ and $d_{O–O}$). This alters the hybridization between M−*d* and O-*p* orbitals, modifying the filling of antibonding orbitals and affecting charge transfer due to electronegativity differences between M''–C and M'–C bonds [41]. These findings suggest that the HER performance of DTM MXenes can be tuned beyond the mono-M MXenes because of the optimized control over electronic states, which enhances hydrogen binding and charge transfer and increases the number of active sites for hydrogen adsorption. Before we further focus on the effect of transition metals on HER behavior of MXenes and present a systematic case study on 14 compositions of M_2CT_x, $M_3C_2T_x$ and $M_4C_3T_x$ MXenes, we first summarize the six major players in controlling the HER performance of MXenes (Fig. 4**a**).

Six key variables in MXenes HER

1. Effect of transition metal (M)

The high density of states near the Fermi level and the unique properties of MXenes, derived from the open *d*-orbitals of transition metals, can be tailored by changing the transition metal (M) to control

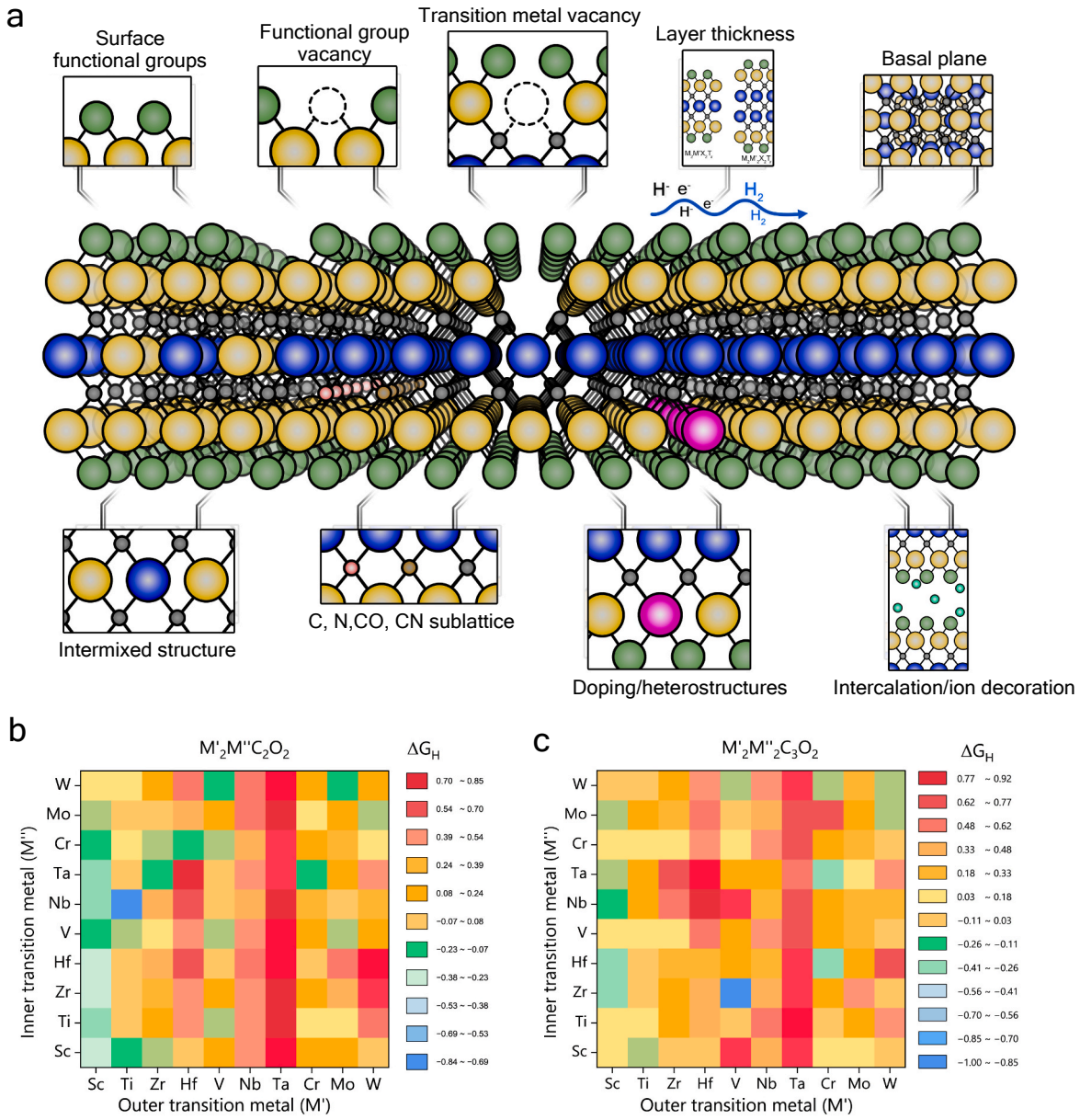

Fig. 4. HER performance kinetics in MXenes. **a** Strategies to tune the MXene properties for enhancing HER performance. Computational prediction of Gibbs free energy distribution for adsorbed hydrogen by DTM MXenes with O-terminations **b** $M'_2M''C_2O_2$ and **c** $M'_2M''_2C_2O_2$ Figure adapted with permission from: **b,c** ref [41].

and enhance HER [40]. Thus, the choice of transition metal in M layers of MXenes plays a crucial role in determining their adsorption efficiency for catalytic reactions by directly influencing their electronic properties [42,43]. Specifically, the electronic structure of the transition metal in MXenes, particularly the number of *d*-electrons, strongly governs adsorption behavior [40]. For example, MXenes with earlier transition metals (e.g., Ti, V), which have partially filled *d*-orbitals, exhibit moderate ΔG_H for HER. In contrast, MXenes with group 6 transition metals (e.g., Mo, W) tend to have stronger interactions with adsorbates due to their higher density of states near the Fermi level [1]. This enhanced charge transfer makes them particularly effective for HER catalytic reactions. As an example, the molybdenum-based MXenes have shown lower HER overpotentials than *iso*-structure titanium-based MXenes [1].

MXenes with DTM enable fine-tuning of ΔG_H and catalytic activity by boosting the synergistic effects of two transition metals with distinct electronic configurations. In ordered DTM MXenes, both transition metals (M' and M'') contribute to the tunability of HER with M' having more effect than M''(Fig. 4**a**). DFT studies using Bayesian error estimation exchange–correlation functional with van der Waals corrections predicted a lower ΔG_H(−0.09 eV) for $Mo_2VC_2T_x$ MXene as compared to $V_3C_2T_x$ MXene, highlighting the effect of outer transition metal in DTM MXenes [43]. Fig. 4**b, c** represent the Gibbs free energy distribution of hydrogen adsorbed by $M'_2M''C_2$ and $M'_2M''_2C_3$ with –O terminations, identifying 47 and 56 compositions, respectively, with -0.2 eV $< \Delta G_H < 0.2$ eV as potential HER electrocatalysts. For example, ΔG_H values of Mo-based MXenes ($Mo_2VC_2O_2$, $Mo_2NbC_2O_2$, and $Mo_2TaC_2O_2$) are closer to 0 eV than their Cr-based MXene counterparts ($Cr_2VC_2O_2$, $Cr_2NbC_2O_2$, and $Cr_2TaC_2O_2$), indicating a better HER activity of the Mo-based MXenes [44].

The effect of the inner metal (M'' in DTM MXenes) is less explored than the outer transition metal, however, M'' also influences the HER [43]. For instance, in a recent experimental study on Mo-based MXenes $Mo_2M''_2C_3T_x$, we showed that change of the inner M from Ti to Nb ($Mo_2Ti_2C_3T_x$ to $Mo_2Nb_2C_3T_x$) leads to more enhanced catalytic activity

for HER with a lower overpotential (~275 mV to ~183 mV, respectively, at 10 mA/cm^2) [23], which is consistent with theoretical predictions [43]. Out of the computationally studied ordered DTM MXenes, only 4 have been synthesized and experimentally studied for HER. This highlights the vast compositional space for further exploration of DTM MXenes for HER electrocatalysis, which is one of the main focus areas of our research group.

Beyond the change of M in the core $M_{n+1}X_n$, introducing early-to-late transition metal adatoms on MXenes induces electron redistribution, enhancing HER activity by changing the charge state on oxygen and facilitating charge transfer for hydrogen, achieving $\Delta G_H < 0.1$ eV and increased HER active sites [45,46]. A high-throughput first-principles study using Perdew–Burke–Ernzerhof functionals on the effect of adatoms on MXene ($M-M_2XO_2$) combinations revealed improvements in HER properties, with some $M-M_2XO_2$ combinations (for example, osmium-Ta_2CO_2, iridium-Sc_2CO_2, tungsten-Nb_2NO_2 with ΔG_H close to 0 eV) switching from the Volmer-Heyrovsky to the Volmer-Tafel reaction pathways [45]. Experimentally, various methods such as cobalt-modified Mo_2Ga_2C precursor for cobalt-Mo_2CT_x [47], molten salt-assisted etching of MAX phases (cobalt-$Ti_3C_2T_x$ using $CoCl_2$ salt [48], and solution-based salt mixing (vanadium, chromium, molybdenum, and manganese salts with $Ti_4N_3T_x$ MXene [49] are used to enhance MXenes HER performance.

2. Effect of X sublattice

MXenes with nitrogen (N) at the X sites exhibit stronger M−X bonding due to nitrogen's higher electronegativity than carbon, resulting in shorter M−M and M−X interatomic distances [40]. This leads to smaller lattice constants, thinner monolayers, and higher in-plane Young's modulus. For instance, $Ti_{n+1}N_nT_x$ MXenes have notably a higher density of states at the Fermi level than $Ti_{n+1}C_nT_x$ MXenes, with predicted higher electrical conductivity and enhanced HER catalytic activity [50,51]. The presence of N in the X sublattice of MXenes promotes lower adsorption energy for hydrogen and facilitates the desorption of hydrogen atoms due to the high density of electronic states, resulting in more active surface chemistry [50,51].

However, synthesizing nitride MXenes is challenging due to the high formation energy of the parent nitride MAX phases, instability of M−N layers in the etchants, and the phase purity [40,52]. While using molten salt or mixed potassium fluoride and hydrochloric acid $Ti_4N_3T_x$ and Ti_2NT_x MXenes are reported, high-yield synthesis of quality MXene flakes remains a challenge [52,53]. Additionally, ammoniation of carbide MXenes, such as converting Mo_2CT_x to Mo_2NT_x and V_2CT_x to V_2NT_x, results in higher electrical conductivity, which is crucial for efficient HER catalysis [54]. Ammoniation has also been used to reduce transition metal oxides to 2D metallic V_2N, MoN, and W_2N [55]. While the resulting phases differ from MXenes, this method can synthesize 2D transition metal nitride and avoid the challenges of nitride MXene synthesis routes.

Unlike the nitride challenges, carbonitride MXenes are more stable, and the carbon and nitrogen solid solution formation in the X sublattice (CN) (Fig. 4**a**) provides opportunities to tune MXenes behavior [56]. Mono-M carbonitride MXenes have been synthesized through controlled processes that balance carbon and nitrogen content, optimizing their HER catalytic properties [57]. DFT studies using Perdew–Burke–Ernzerhof functionals on carbonitride M_3CNO_2 (M = Ti, V, Cr, Zr, Nb, Mo, Hf, Ta) predicted Ti_3CNO_2 and Nb_3CNO_2 have low overpotentials for HER with ΔG_H values of −0.122 eV and −0.117 eV, respectively [58]. A few experimental studies have investigated Ti_3CNO_2 MXenes for electrocatalysis, demonstrating the lower overpotential of ~148 mV at 10 mA/cm^2 for HER [57].

Similarly, HER activity of various DTM carbonitrides $M'_2M''CNO_2$ (M' = Ti, V, Cr, Zr, Nb, Mo, Hf, Ta; M'' = Ti, V, Cr, Zr, Nb, Mo, Hf, Ta) was studied theoretically, identifying candidates with Pt-like activity [58]. Ti_2NbCNO_2, Mo_2TiCNO_2, and Ti_2VCNO_2 were found to be particularly stable, showing exceptional promise due to ΔG_H values close to 0.02 eV [58]. These studies suggest the presence of two metals combined with two X, that is, ordered DTM carbonitride MXenes, might provide the best tunability of the electronic structure to achieve the best HER performance in MXenes.

3. Effect of surface terminations (T_x)

The composition of surface terminations is highly dependent on the synthesis method, particularly the etchants and the type of metal species in MXenes, which governs the stability of the M−T_x interaction [2,34,40]. Studies indicate that MXenes with surface terminations (Fig. 4**a**) exhibit better catalytic performance than bare MXenes (i.e., MXenes with no surface termination) [34]. The substantial negative formation energy of T_x underscores the strong interaction between M atoms and terminating groups, which modifies the electronic structure of MXenes and the *d*-band center of the transition metal, further enhancing hydrogen absorption and desorption [34].

Surface termination chemistry, while less explored, has a major role in the HER performance of MXenes. For example, higher content of –F in F-terminated Mo- and Ti-based MXenes was found to decrease the HER catalytic performance [32], and consequently tailoring MXene synthesis conditions to reduce –F terminations is desired for HER [32,40]. MXenes with –OH terminations, despite having poorer oxidation stability, may offer advantages in HER photocatalysis [59]. Specifically, the edges of $Ti_3C_2(OH)_2$ MXene flakes are prone to converting into highly active TiO_2, enhancing photocatalytic activity and increasing hydrogen production yield [59]. MXenes with –O terminations exhibit superior HER performance compared to –F terminations due to several factors [34,60]. The –O terminations create stronger and more favorable hydrogen binding sites, enhancing adsorption and desorption processes. They also improve the electronic structure by increasing the density of states near the Fermi level, boosting electron transfer rates. The hydrophilicity of O-terminated MXenes promotes better water interaction, facilitating efficient proton transfer and enhancing catalytic efficiency [34].

The coverage percentage and position of the surface terminations are also important for HER. DFT studies using Perdew–Burke–Ernzerhof functionals indicate that MXenes with 100 % –O surface coverage have enhanced HER performance [44]. Out of two primary adsorption sites for surface terminations [43,44,58], surface –O terminations positioned above the C-atom of the outermost C layer (*hcp*, as opposed to above the inner M metals, *fcc*) are predicted to boost HER performance [44]. This improvement is due to better electronic structure modifications, increased density of states near the Fermi level, enhanced electron transfer rates, and more active catalytic sites, promoting efficient proton transfer and stronger water interaction [44].

The stability of MXene surface terminations (–O, –OH, –F) under HER conditions is highly dependent on electrochemical potential and pH, as demonstrated by computational Pourbaix diagrams [61]. These studies reveal that mixed surface terminations are thermodynamically more stable than single terminations under HER equilibrium conditions. Moreover, mixed terminations synergistically enhance HER activity by optimizing ΔG_H and tuning electronic properties through position (*hcp, fcc*) specific interactions [62]. These findings are crucial for bridging the gap between theoretical studies and practical catalyst design.

Recent advancements in MXene synthesis, such as molten-salt synthesis, have introduced new functional groups, such as –Cl, –Br, and –I [27]. These can be further exchanged with ligands, such as –NH, –S, −Se, and −Te, via processes involving lithium salts [63]. The molten salt synthesized Cl-terminated MXene has shown enhanced HER performance compared to F-terminated ones made via HF etching routes, possibly due to the negative impact of flourine termination on MXene HER activity [32] along with less defective surfaces of MXene made via molten salt from high-temperature synthesis [64]. These findings highlight the critical role of the less explored surface terminations, their

compositions, adsorption sites, and coverage in optimizing MXenes for hydrogen production.

4. Effect of 2D flake thickness, lateral size, and stacking

The stability and properties of MXenes, including HER activity, are influenced by MXene flake thickness with $n = 1$–4 (Fig. 1). DFT studies using Perdew–Burke–Ernzerhof functionals indicate that ΔG_H and electronic structures vary with thickness. For example, $Ti_3C_2T_x$ has lower electrical resistivity than Ti_2CT_x due to easier electron hopping in $Ti_3C_2T_x$ [42]. Specifically, ΔG_H can differ by > 0.5 eV between MXenes with two vs. four metal layers ($n = 1$ and 3). However, there is no clear trend in adsorption energies based on MXene layer thickness. For example, in vanadium carbides, the adsorption energy decreases as the thickness increases, while niobium and tantalum carbides, which belong to the same group as vanadium, do not show a similar trend [42].

Some DFT studies using Perdew–Burke–Ernzerhof functionals indicate that the HER activity of MXenes is dependent on thickness, with ΔG_H approaching $\sim$ 0 eV as thickness decreases [65]. For example, a study on single atomic Pt catalyst decorated-$Ti_{n+1}C_nO_2$ MXene, with $n =$ 1–3, investigated the quantum confinement effect on HER catalytic performance and found Pt decorated-Ti_2CO_2 MXene exhibited a lower $\Delta G_H = +0.01$ eV [65]. In general, the challenge with the thinnest MXenes is their chemical stability as the thinnest MXenes ($n = 1$), such as Ti_2CT_x, are shown to be less chemically stable than thicker MXenes of similar composition (i.e., $Ti_3C_2T_x$) [65].

In addition to flake thickness, MXene flake lateral sizes can affect the HER. MXene flakes with large lateral sizes ($\sim$1 μm) showed the best electrochemical performance with a capacitance of 290 F/g at 2 mV/s [66]. Because MXene basal planes (flake surfaces) are electrocatalytically active [1], larger MXene flakes offer more active sites, boosting catalytic efficiency. Smaller flakes introduce more edges and defects, which can affect HER performance. However, the effect of different MXene flake sizes on HER remains unexplored.

Experimental studies have also highlighted the effect of the number of stacked MXene flakes (multilayer vs. single-to-few-layer) on their HER activity [1]. Single-to-few-layer MXene flakes show an increase in the exposed basal plane surface area, which enhances their HER activity. A study on Mo_2CT_x MXene flake stacking revealed that fewer stacked flakes enhance HER activity due to more active catalytic sites [33].

5. Effect of defects

Atomic vacancies (such as carbon and transition metal vacancies) and edge defects are intrinsic defects that increase active site density and alter electronic properties [67]. Atomic vacancies and edges can be either created during the MXene selective etching and delamination [46] or originate from the precursor (e.g., vacancies in the MAX phase or its grain boundaries). It has been shown that atomic-level transition metal vacancies in MXenes can be controlled by varying the concentration of etchants and quantified using STEM or atomic-layer resolution secondary ion mass spectrometry [68,69]. Control and understanding the point defects (vacancies) are critical for HER, which is also underexplored.

DFT studies using Perdew–Burke–Ernzerhof functionals indicated that the random distribution of vacancies of carbon and transition metal enhances the HER activity of M_2CO_2 MXenes by optimizing O–H bonding [70]. The vacancies shift the Fermi level, altering the strength of O–H interactions. In some compositions, e.g., Ti_2CO_2, W_2CO_2, Nb_2CO_2, and Ta_2CO_2 with strong O–H bonding, carbon vacancies alone can improve HER activity. Still, in V_2CO_2, Cr_2CO_2, Zr_2CO_2, and Hf_2CO_2 with weaker O–H binding, the presence of both carbon and transition metal vacancies is required to enhance HER performance [70]. Introducing atomic vacancies cannot always enhance the HER. Comparing experimental investigations on $Mo_{1.33}CT_x$ and Mo_2CT_x MXenes reveals lower HER activity in $Mo_{1.33}CT_x$ due to ordered divacancies affecting carbon and oxygen coordination and hindering hydrogen adsorption [71]. To optimize the surface terminations on a divacancy MXene, another ordered divacancies MXene, $W_{1.33}CT_x$, was annealed ($\sim$700 °C for 1 h) in an inert atmosphere, which led to improved HER performance (change of overpotential from $\sim$580 mV to $\sim$320 mV at 10 mA/cm^2 after annealing) [72].

Edge defects in MXenes, originating from 2D flake boundaries and pores as well as the precursor grain boundaries, are less explored but hold potential for controlling the HER performance. The edges can potentially provide a high density of active sites, but increasing the edges leads to smaller flake sizes (smaller basal plane areas), which can lower the HER. In general, more edge defects can be made by downsizing MXenes to smaller flakes and even zero dimensional (0D) nanostructures through harsh etching, delamination, or post-processing conditions. For instance, a study demonstrated that nanostructuring MXene into 0D nanodots created more active edge sites, improving HER performance [73]. These conflicting studies suggest that MXene intrinsic defects play a crucial role in their HER performance but systematic studies are required to fully understand the underlying mechanisms.

6. Effect of heteroatoms and intercalants

Heteroatom doping (i.e., elements that are not inherent to MXenes) enhances the electrochemical performance of MXenes by introducing new active sites, altering the electronic structure, and improving adsorption capacity [74–77]. The position of heteroatoms is crucial (attached to the surface or go into the metal vacancy sites). Transition metal vacancies created during MXene synthesis can trap heteroatoms, stabilizing them through charge transfer between the transition metal species and vacancy defect sites. For instance, DTM $Mo_2TiC_2T_x$ MXene synthesis by electrochemical exfoliation creates molybdenum vacancies that have been explored to immobilize single Pt atoms [75]. The resulting Pt-$Mo_2TiC_2T_x$ MXene exhibits higher HER catalytic activity with a mass activity 40 times greater than commercial Pt/C due to strong covalent interactions between Pt atoms and the $Mo_2TiC_2T_x$ MXene [75].

Additionally, doping with non-metal heteroatoms (e.g., B, N, O, P, S) tailors the surface chemistry of MXenes, accelerates electron/ion transport, and increases active sites, promoting HER activity [76]. DFT studies using Perdew–Burke–Ernzerhof functionals indicate that Ti_2CO_2 doped with various non-metal atoms (B, C, N, O, F) optimized conductivity and improved HER activity [76]. Experimental studies have confirmed these theoretical predictions [78]. For instance, N-doping in Ti_2CT_x increased stability and exhibited superior HER activity, with a low overpotential of 215 mV at 10 mA/cm^2, outperforming pristine Ti_2CT_x [78]. In another example, doping V_2CT_x MXenes with P creates P-carbon bonds, which serve as active sites, effectively balancing the energy barriers for H^+ reduction and H* desorption, thereby enhancing HER kinetics [77]. Additionally, ammonia heat treatment for nitrogen doping in $Ti_3C_2T_x$ MXenes incorporates various N species, enhancing electrical conductivity and catalytic reactivity [79]. This results in a lower overpotential of 198 mV at 10 mA/cm^2, outperforming pristine $Ti_3C_2T_x$ MXenes [79].

Intercalation and interactions of multivalent cations, water, and organic molecules can also tailor MXene HER catalysis by delamination, attachment to MXene surfaces, and altering the inter-layer spacing [31,80]. Intercalating ions with smaller sizes and higher valence states increase the intercalation capacity but exhibit more considerable diffusion barriers. The intercalation process and resulting properties of MXenes depend on the varying electronegativities of the M, X, and T_x, which influence electron distribution, atomic interaction strength, and lattice parameters [80]. For instance, MXenes intercalated with organic molecules like dimethyl sulfoxide (DMSO) and tetrabutylammonium hydroxide (TBAOH) and cations like lithium are reported for HER studies [80]. Overall, the impact of heteroatom doping, molecule attachments and hetertostructuring with other materials [81] on HER is worth exploring, as the current literature is very limited.

Effect of M composition on HER of 14 MXenes

Motivated by computational studies and limited experimental investigations on the effect of basal plane transition metals on HER, one of the focus areas in our research lab is investigating the effect of different M on MXenes HER. After presenting the six variables in HER performance, we end this article by presenting a systematic HER evaluation of single-metal and ordered double metal MXenes. We study four M_2CT_x (Mo_2CT_x, V_2CT_x, Nb_2CT_x and Ti_2CT_x), four $M_3C_2T_x$ ($Ti_3C_2T_x$, $Mo_2TiC_2T_x$, $Cr_2TiC_2T_x$ and $W_2TiC_2T_x$) and six $M_4C_3T_x$ ($V_4C_3T_x$, $Nb_4C_3T_x$, $Ta_4C_3T_x$, $Mo_2Ti_2C_3T_x$, $Mo_2Nb_2C_3T_x$ and $Mo_2V_2C_3T_x$) MXenes. We used an identical etching and delamination route for their synthesis from their precursors Mo_2Ga_2C, V_2AlC, Nb_2AlC, Ti_2AlC, Ti_3AlC_2, Mo_2TiAlC_2, Cr_2TiAlC_2, $(W,Ti)_4C_{4-y}$, V_4AlC_3, Nb_4AlC_3, Ta_4AlC_3, $Mo_2Ti_2AlC_3$, $Mo_2Nb_2AlC_3$, and $Mo_2V_2AlC_3$ (Fig. 5). We characterized the synthesized precursors and resulting MXenes using XRD and SEM characterization (**ESI,** Fig. S2, S3, and S4).

We compare their HER behavior (Fig. 6) and details of their electrochemical HER measurements are described in the SI. For M_2CT_x MXenes (Fig. 6**a**), Mo_2CT_x MXene showed the lowest overpotential of 196 ± 8 mV at 10 mA/cm^2, which is 2.4-fold lower than Ti_2CT_x MXene (482 ± 12 mV). For $M_3C_2T_x$ MXenes (Fig. 6**b**), $W_2TiC_2T_x$ MXene showed the lowest overpotential of 149 ± 6 mV at 10 mA/cm^2, which is 3.4-fold lower than $Ti_3C_2T_x$ MXene (510 ± 10 mV). $W_2TiC_2T_x$ was followed by $Mo_2TiC_2T_x$ and $Cr_2TiC_2T_x$ at 243 ± 19 mV and 275 ± 11 mV, respectively (Fig. 6**b**). For $M_4C_3T_x$ MXenes (Fig. 6**c**), $Mo_2Nb_2C_3T_x$ MXene showed the lowest overpotential of 189 ± 7 mV at 10 mA/cm^2, which is 2.2-fold lower than $Ta_4C_3T_x$ MXene (415 ± 15 mV). We also map the trend in the measured overpotentials for the 14 MXenes screened in this study (Fig. 6**d,** Table S2). Among all tested MXenes, $W_2TiC_2T_x$ MXene shows the lowest overpotential of ~149 mV at 10 mA/cm^2, which is still 3.7-fold higher as compared to benchmark Pt/C (~40 mV at 10 mA/cm^2) under acidic conditions. This improving trend in MXenes HER agrees with reported computational studies, which show that HER activity of MXenes is attributed to the active basal plane of transition metal and lower ΔG_H [44].

The Tafel slope was determined from the LSV plot (**ESI,** Fig. S5) to gain deeper insights into the electrocatalytic HER reaction kinetics. The Tafel slope of ~70 mV/dec observed for $W_2TiC_2T_x$ indicates that the HER process follows the Volmer-Heyrovsky mechanism. This mechanism involves a rapid initial Volmer discharge step followed by a slower electrochemical desorption Heyrovsky step. This observation indicates that $W_2TiC_2T_x$ possesses more electrochemically active sites, enhancing the electrochemical HER performance due to a dominant influence from W on MXene basal planes. Additionally, $W_2TiC_2T_x$ MXene tends to have stronger interactions with adsorbates due to their higher density of states near the Fermi level [1,40]. This enhanced charge transfer makes them potential candidates for HER catalytic reactions. The stability of $W_2TiC_2T_x$ MXene was evaluated under acidic conditions, which confirmed its stable aqueous performance (**ESI,** Fig. S6). This systematic study shows a correlation between the experimental HER overpotentials and the effect of transition metals in the basal plane ranging from single-metal, ordered double-metal, and four-metal MXenes. This provides insights into the role of the outer transition metal in M_2CT_x, $M_3C_2T_x$ and $M_4C_3T_x$ MXenes influencing their HER catalytic performance.

Conclusion and outlook

This article illustrates MXenes as promising catalyst materials for HER electrocatalysis and outlines six key factors that govern their tunability: composition (M, X, and T_x), flake thickness (number of atomic layers), lateral flake dimensions, surface adatoms and intercalants, atomic defects (e.g., vacancies), and heteroatom doping. Each parameter plays a critical role in controlling the catalytic activity of MXenes by tailoring the electronic structure, adsorption energetics, and surface reactivity. For instance, fine-tuning of ΔG_H and electronic configuration in MXenes enhance HER through: (i) high density of states near the Fermi level of transition metals, (ii) incorporation of two or more transition metals and X elements with distinct electronic structures, (iii) tunable surface terminations (–O, –OH, –F, –Cl) and site-specific coverage, and (iv) control of atomic defect at M or X sites. Additionally, flake thickness and lateral dimensions enhance basal plane exposure which improves HER activity, while intercalants, adatoms or dopants adjust interlayer spacing and charge transport pathways. Future investigations should systematically study the effects of varying transition metals and X elements, synthesis methods, flake sizes, defects, and surface modifications to optimize HER performance and advance MXene applications in sustainable energy technologies.

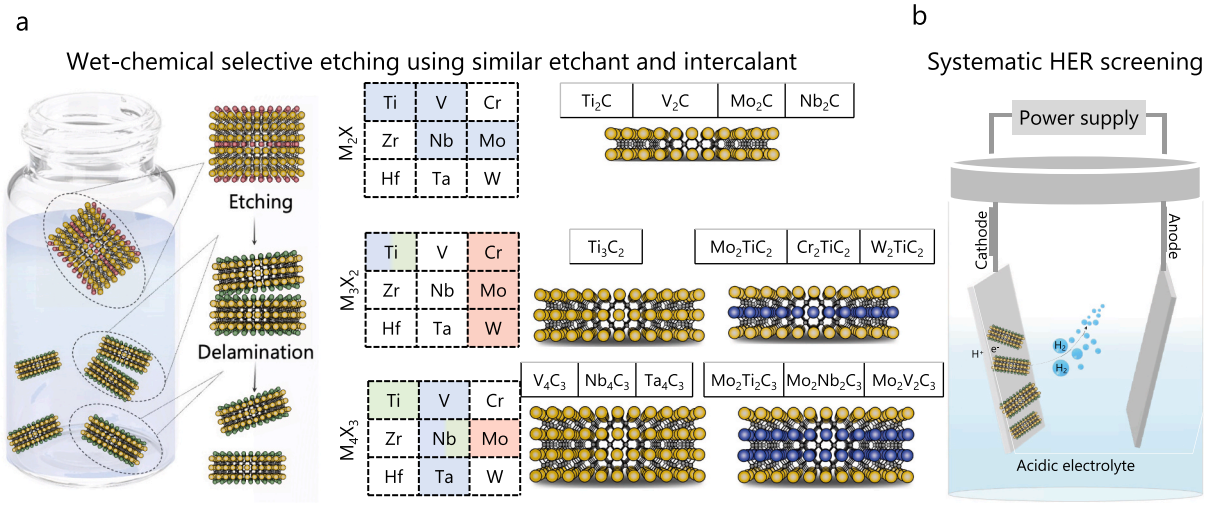

Fig. 5. Schematic for the systematic synthesis of MXenes in this study and their electrocatalysis. **a** Selective etching of the Al layers in MAX phases/precursor followed by delamination process to synthesize single-to-few layered four M_2CT_x (Mo_2CT_x, V_2CT_x, Nb_2CT_x and Ti_2CT_x), four $M_3C_2T_x$ ($Ti_3C_2T_x$, $Mo_2TiC_2T_x$, $Cr_2TiC_2T_x$ and $W_2TiC_2T_x$) and six $M_4C_3T_x$ ($V_4C_3T_x$, $Nb_4C_3T_x$, $Ta_4C_3T_x$, $Mo_2Ti_2C_3T_x$, $Mo_2Nb_2C_3T_x$, and $Mo_2V_2C_3T_x$ MXenes. Elements used in this study to synthesize M_2X MXenes (blue background for M layers), M_3X_2 and M_4X_3 MXenes (blue background for monometal M layers, green background for inner M layers in DTM MXenes and red background for outer M layers in DTM MXenes). The surface teminations T_x are not shown for simplicity. **b** Illustration of the systematic approach followed for screening synthesized MXenes in the acidic electrolyte for electrocatalytic hydrogen evolution reaction. (For interpretation of the references to colour in this figure legend, the reader is referred to the web version of this article.)

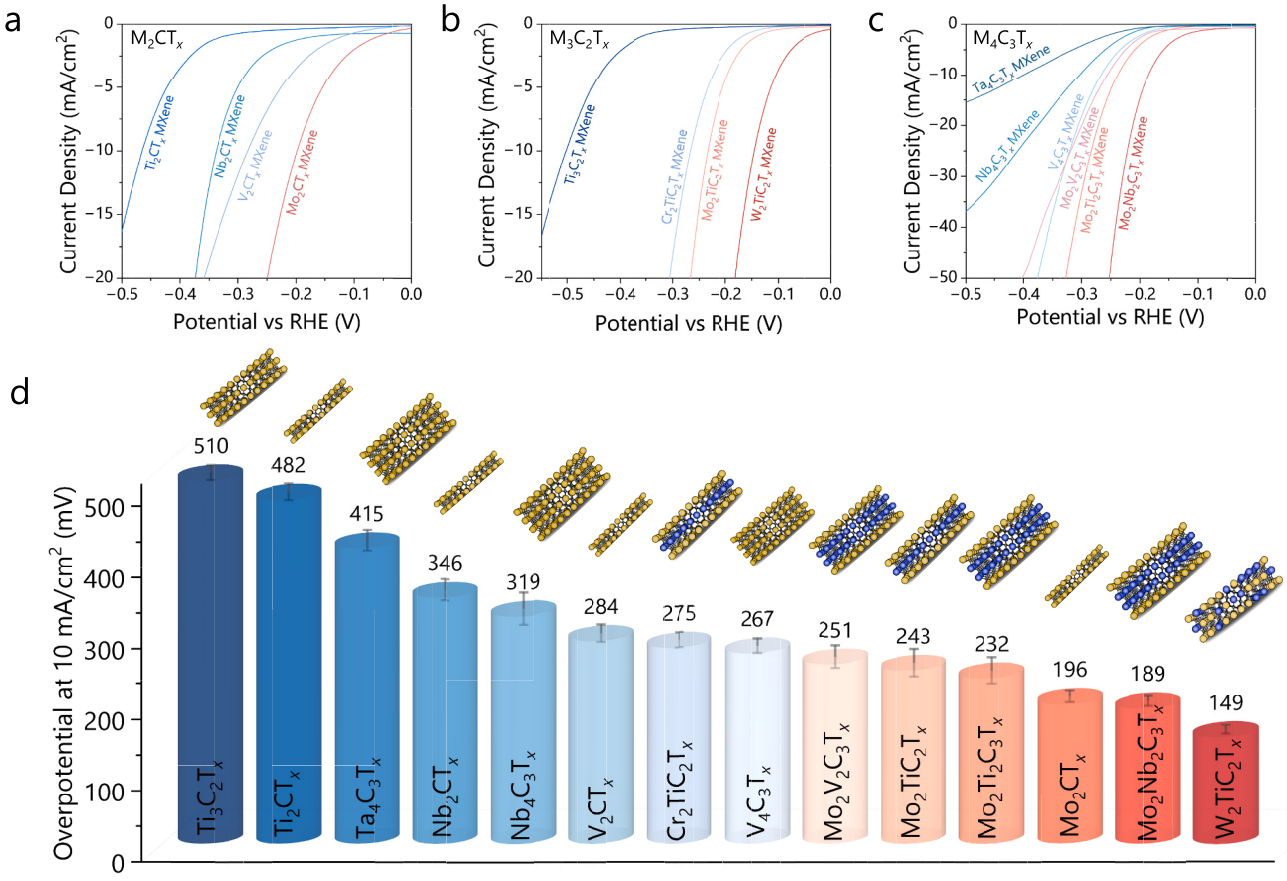

Fig. 6. Electrochemical HER performance of MXenes synthesized and tested under similar conditions in this study. Linear sweep voltammetry plot measured in Ar-bubbled 0.5 M H_2SO_4 electrolyte for **a** M_2CT_x, **b** $M_3C_2T_x$, and **c** $M_4C_3T_x$ MXenes. **d** Experimental overpotentials measured at a current density of 10 mA/cm^2.

One of the key factors influencing MXenes HER is their transition metal compositions. To systematically evaluate this effect, we focused on the role of the outer transition metal on the HER activity of 14 M_2CT_x, $M_3C_2T_x$ and $M_4C_3T_x$ MXenes. We synthesized four M_2CT_x (Mo_2CT_x, V_2CT_x, Nb_2CT_x, Ti_2CT_x), four $M_3C_2T_x$ ($Ti_3C_2T_x$, $Mo_2TiC_2T_x$, $Cr_2TiC_2T_x$, $W_2TiC_2T_x$) and six $M_4C_3T_x$ ($V_4C_3T_x$, $Nb_4C_3T_x$, $Ta_4C_3T_x$, $Mo_2Ti_2C_3T_x$, $Mo_2Nb_2C_3T_x$, $Mo_2V_2C_3T_x$) MXenes under similar etching and delamination conditions. Their HER performance was compared and $W_2TiC_2T_x$ exhibited the lowest HER overpotential (~149 mV at 10 mA/cm^2) under acidic conditions, outperforming the other MXenes. This enhanced HER activity is likely due to presence of tungsten as the main outer transition metal. These findings highlight the importance of transition metal composition in the basal plane on MXene catalytic activity.

Looking ahead, the findings from this study open up multiple avenues for further expanding the landscape of MXene-based electrocatalysts. One promising direction is the control of surface terminations, which remains relatively underexplored. Future research should investigate surface modification strategies to fine-tune surface terminations and ΔG_H optimization. Likewise, atomic-level defect engineering in MXenes holds potential for increasing the density of catalytically active sites. In addition, the design of MXene-based hybrids with other nanomaterials may enhance charge transfer and mass transport. Furthermore, the use of *in-situ* electrochemical techniques, theory-guided catalyst design, and the integration of high-throughput computational screening, machine learning, and artificial intelligence will be critical to accelerating the tunable design of MXenes for sustainable energy applications.

CRediT authorship contribution statement

Anupma Thakur: Writing – review & editing, Writing – original draft, Visualization, Methodology, Investigation, Conceptualization. **Nithin Chandran B.S.:** Writing – review & editing, Visualization, Methodology, Investigation. **Brian C. Wyatt:** Writing – review & editing, Investigation. **Annabelle Bedford:** Writing – review & editing, Investigation. **Mostafa Dadashi Firouzjaei:** Writing – review & editing, Visualization. **Krutarth Kamath:** Writing – review & editing, Investigation. **Muhammad Sharif Uddin:** Writing – review & editing, Investigation. **Babak Anasori:** Writing – review & editing, Visualization, Supervision, Methodology, Conceptualization.

Declaration of competing interest

The authors declare that they have no known competing financial interests or personal relationships that could have appeared to influence the work reported in this paper.

Acknowledgments

The authors acknowledge the support from the National Science Foundation for funding this project under the Center for Chemical Innovation (NSF CCI) program grant 2318105. The authors also acknowledge Srinivas Kartik Nemani for his valuable comments in improving the manuscript.

Appendix A. Supplementary data

Details of HER kinetics and mechanisms in MXenes. The experimental section includes materials and methods for synthesizing starting MAX phase/precursor (Mo_2Ga_2C, V_2AlC, Nb_2AlC, Ti_2AlC, Ti_3AlC_2, Mo_2TiAlC_2, Cr_2TiAlC_2, $(W,Ti)_4C_{4-y}$, V_4AlC_3, Nb_4AlC_3, Ta_4AlC_3, $Mo_2Ti_2AlC_3$, $Mo_2Nb_2AlC_3$, $Mo_2V_2AlC_3$, and their derived MXenes (Mo_2CT_x, V_2CT_x, Nb_2CT_x, Ti_2CT_x, $Ti_3C_2T_x$, $Mo_2TiC_2T_x$, $Cr_2TiC_2T_x$, $W_2TiC_2T_x$, $V_4C_3T_x$, $Nb_4C_3T_x$, $Ta_4C_3T_x$, $Mo_2Ti_2C_3T_x$, $Mo_2Nb_2C_3T_x$, $Mo_2V_2C_3T_x$ MXenes). Material characterization of MAX/precursor and MXenes using XRD and FESEM and Tafel slope analysis. Supplementary data to this article can be found online at https://doi.org/10.1016/j.mattod.2025.06.018.

Data availability

Data will be made available on request.

References

[1] Z.W. Seh, et al., ACS Energy Lett. 1 (3) (2016) 589.
[2] K.R.G. Lim, et al., ACS Nano 14 (9) (2020) 10834.
[3] K.R.G. Lim, et al., Nat. Synth. 1 (8) (2022) 601.
[4] Y. Gogotsi, B. Anasori, ACS Nano 13 (2019) 8491.
[5] M. Sokol, et al., Trends Chem. 1 (2) (2019) 210.
[6] A. VahidMohammadi, et al., Science 372 (6547) (2021) eabf1581.
[7] A. Thakur, et al., Small Methods 7 (2023) 2300030.
[8] B.C. Wyatt, et al., J. Phys. Condens. Matter 33 (22) (2021) 224002.
[9] A. Morales-Garcia, et al., ACS Catal. 10 (22) (2020) 13487.
[10] S. Bai, et al., npj 2D Mater. Appl. 5 (1) (2021) 78.
[11] B. Anasori, et al., ACS Nano 9 (10) (2015) 9507.
[12] I. Persson, et al., Small 14 (17) (2018) 1703676.
[13] G. Deysher, et al., ACS Nano 14 (1) (2020) 204.
[14] S.K. Nemani, et al., ACS Nano 15 (8) (2021) 12815.
[15] W. Hong, et al., MRS Bull. 45 (10) (2020) 850.
[16] M. Han, et al., J. Am. Chem. Soc. 142 (45) (2020) 19110.
[17] B. Anasori, et al., J. Appl. Phys. 118 (2015) 9.
[18] R. Meshkian, et al., Acta Mater. 125 (2017) 476.
[19] K. Hantanasirisakul, et al., Nanoscale Horiz. 5 (12) (2020) 1557.
[20] A. Thakur, et al., Nat. Synth. 1 (2025) 13.
[21] W. Liu, et al., Rare Met. 42 (1) (2023) 100.
[22] X. Feng, et al., Mater. Sci. Eng. B 305 (2024) 117403.
[23] B.C. Wyatt, et al., Nano Lett. 23 (3) (2023) 931.
[24] D. Maldonado-Lopez, et al., ACS Appl. Nano Mater. 5 (2) (2022) 1801.
[25] B. Wyatt, et al., ChemRxiv. (2025).
[26] T. Zhang, et al., Chem. Mater. 36 (4) (2024) 1998.
[27] H. Ding, et al., Science 379 (6637) (2023) 1130.
[28] L. Liu, et al., Electrochem. Commun. 148 (2023) 107453.
[29] D. Wang, et al., Science 379 (6638) (2023) 1242.
[30] M. Xiang, et al., The Innovation 5 (1) (2024) 100540.
[31] J. Zou, et al., Chem. Soc. Rev. 51 (8) (2022) 2972.
[32] A.D. Handoko, et al., ACS Appl. Energy Mater. 1 (1) (2017) 173.
[33] J. Wu, et al., Adv. Mater. 35 (25) (2023) 2209954.
[34] B. Miao, et al., Renew. Sustain. Energy Rev. 199 (2024) 114506.
[35] A. Thakur, et al., MRS Energy & Sustainability (2025).
[36] J. Greeley, et al., Nat. Mater. 5 (11) (2006) 909.
[37] H. Wang, et al., Nano Res. 8 (2015) 566.
[38] L. Meng, et al., Curr. Opin. Electrochem. (2023) 101332.
[39] G. Gao, et al., ACS Catal. 7 (1) (2017) 494.
[40] A.D. Handoko, et al., Nanoscale Horiz. 4 (4) (2019) 809.
[41] X. Wang, et al., J. Mater. Chem. A 8 (44) (2020) 23488.
[42] M. Pandey, K.S. Thygesen, J. Phys. Chem. C 121 (25) (2017) 13593.
[43] D. Jin, et al., J. Phys. Chem. C 124 (19) (2020) 10584.
[44] N. Li, et al., ACS Omega 6 (37) (2021) 23676.
[45] P. Li, et al., J. Mater. Chem. A 6 (10) (2018) 4271.
[46] Y. Tang, et al., Adv. Energy Mater. 12 (12) (2022) 2103867.
[47] D.A. Kuznetsov, et al., J. Am. Chem. Soc. 141 (44) (2019) 17809.
[48] R. Luo, et al., Int. J. Hydrogen Energy 46 (64) (2021) 32536.
[49] A. Djire, et al., Adv. Funct. Mater. 30 (47) (2020) 2001136.
[50] N. Zhang, et al., 2D Mater. 5 (4) (2018) 045004.
[51] G.R. Berdiyorov, Europhys. Lett. 111 (6) (2015) 67002.
[52] B. Soundiraraju, B.K. George, ACS Nano 11 (9) (2017) 8892.
[53] P. Urbankowski, et al., Nanoscale 8 (22) (2016) 11385.
[54] P. Urbankowski, et al., Nanoscale 9 (45) (2017) 17722.
[55] X. Xiao, et al., ACS Nano 11 (2) (2017) 2180.
[56] T. Zhang, et al., J. Am. Chem. Soc. 145 (41) (2023) 22374.
[57] K. Liang, et al., Mater. Rep.: Energy 2 (1) (2022) 100075.
[58] Z. Zeng, et al., npj Comput. Mater. 7 (1) (2021) 80.
[59] X. Xie, N. Zhang, Adv. Funct. Mater. 30 (36) (2020) 2002528.
[60] T. Su, et al., J. Mater. Chem. A 10 (19) (2022) 10265.
[61] M. López, et al., Adv. Theor. Simul. 6 (10) (2023) 2200217.
[62] L. Meng, et al., J. Mater. Chem. A 11 (13) (2023) 6886.
[63] V. Kamysbayev, et al., Science 369 (6506) (2020) 979.
[64] B. Sarfraz, et al., Int. J. Energy Res. 46 (8) (2022) 10942.
[65] Z. Shu, Y. Cai, J. Phys. Condens. Matter 35 (20) (2023) 204001.
[66] K. Maleski, et al., ACS Appl. Mater. Interfaces 10 (29) (2018) 24491.
[67] Q. Tao, et al., Nat. Commun. 8 (1) (2017) 14949.
[68] B.C. Wyatt, et al., Nat. Commun. 15 (1) (2024) 6353.
[69] X. Sang, et al., ACS Nano 10 (10) (2016) 9193.
[70] J. Gan, et al., The Journal of Physical Chemistry Letters 12 (20) (2021) 4805.
[71] S. Intikhab, et al., J. Catal. 371 (2019) 325.
[72] R. Meshkian, et al., Adv. Mater. 30 (21) (2018) 1706409.
[73] D.N. Nguyen, et al., ACS Nano 14 (12) (2020) 17615.
[74] X. Wu, et al., iScience (2024) **27** (2).
[75] J. Zhang, et al., Nat. Catal. 1 (12) (2018) 985.
[76] X. Wang, et al., Appl. Surf. Sci. 556 (2021) 149778.
[77] Y. Yoon, et al., Adv. Funct. Mater. 29 (30) (2019) 1903443.
[78] Y. Yoon, et al., J. Mater. Chem. A 6 (42) (2018) 20869.
[79] T.A. Le, et al., ACS Sustain. Chem. Eng. 7 (19) (2019) 16879.
[80] J. Jiang, et al., J. Mater. Chem. A 9 (43) (2021) 24195.
[81] J. Jiang, et al., Sci. China Mater. 65 (11) (2022) 2895.